

Synthesis and Study of 2-(Pyrrolesulfonylmethyl)-*N*-arylimines: A New Class of Inhibitors for Human Glutathione Transferase A1-1

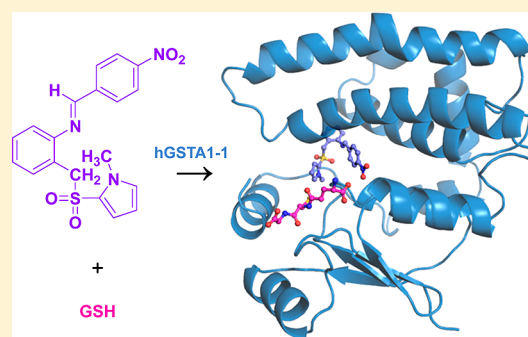
Georgia E. Koutsoumpli,[†] Virginia D. Dimaki,[§] Trias N. Thireou,[‡] Elias E. Eliopoulos,[‡] Nikolaos E. Labrou,[†] George I. Varvounis,^{*,§} and Yannis D. Clonis^{*,†}

[†]Laboratory of Enzyme Technology and [‡]Laboratory of Genetics, Department of Agricultural Biotechnology, Agricultural University of Athens, 75 Iera Odos Street, GR-118 55 Athens, Greece

[§]Section of Organic Chemistry and Biochemistry, Department of Chemistry, University of Ioannina, GR-451 10 Ioannina, Greece

S Supporting Information

ABSTRACT: Overexpression of human GSTA1-1 in tumor cells is part of MDR mechanisms. We report on the synthesis of 11 pyrrole derivatives as hGSTA1-1 inhibitors starting from 1-methyl-2-[(2-nitrobenzylsulfanyl)-1*H*-pyrrole]. Molecular modeling revealed two locations in the enzyme H binding site: the catalytic primary one accommodating shorter and longer derivatives and the secondary one, where shorter derivatives can occupy. Derivative **9**, displaying the highest inhibition and bearing a *p*-nitroarylimino moiety, and derivative **4**, lacking this moiety, were studied kinetically. Derivative **9** binds ($K_{i(9)} = 71 \pm 4 \mu\text{M}$) at the primary site competitively vs CDNB. Derivative **4** binds ($K_{i(4)} = 135 \pm 27 \mu\text{M}$) at the primary and secondary sites, allowing the binding of a second molecule (**4** or CDNB) leading to formation of unreactive and reactive complexes, respectively. The arylmethylsulfonylpyrrole core structure is a new pharmacophore for hGSTA1-1, whereas its derivative **9** may serve as a lead structure.



INTRODUCTION

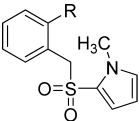
Glutathione *S*-transferases (GSTs, EC 2.5.1.18) are a family of isoenzymes that differ in their tissue-specificity expression and distribution. They catalyze the conjugation of glutathione (GSH) to a variety of hydrophobic endogenous and exogenous substrates, rendering them hydrophilic and facilitating their metabolic processing and eventual secretion from the cell.^{1–4} GSTs are subdivided into classes on the basis of their amino acid sequence, whereas cytosolic ones are found as homodimers or heterodimers.⁵ Each monomer has an α/β domain that includes $\alpha 1$ – $\alpha 3$ helices and a large α -helical domain comprising helices $\alpha 4$ – $\alpha 9$. The former domain contains the GSH binding site (G-site) on top of the large α domain. A hydrophobic pocket (H-site) lies between the two domains in which the hydrophobic substrate binds and reacts with GSH. Since the produced conjugates are susceptible to further modification and eventual secretion from the cell, the GSTs are involved in major detoxification mechanisms of the cell from several xenobiotics and drugs. On the other hand, on the basis of the same detoxification mechanisms, cancer cells may acquire resistance by overexpressing GST activities,^{6,7} thus hampering the effectiveness of certain chemotherapeutic drugs. This mechanism leads to chemotherapeutic resistant tumor cells that no longer respond appropriately to the applied therapeutic protocol.⁸ A plausible mechanism by which GSTs could contribute to drug resistance includes GST-dependent prevention of drug-induced apoptosis via direct interaction with signal transduction proteins, as suggested for GSTP1-1^{9,10}

inhibiting c-Jun *N*-terminal kinase. Furthermore, the *in vitro* resistance to doxorubicin by blast cells, derived from acute myeloid leukemia patients, has been attributed to elevated activity of hGSTA1/A2 enzymes⁶ whereas a correlation *in vitro* has been reported between GST α in gastric cancer tissues and cisplatin resistance.⁷ Interestingly, the death hazard of homozygous hGSTA1*B breast cancer patients treated with cyclophosphamide (plus other chemotherapeutic drugs) was reduced during the first 5 years following diagnosis, compared with homozygous hGSTA1*A individuals (hazard ratio, 0.3).⁹ This observation was attributed to the detoxifying role of hepatic hGSTA1 against therapeutic metabolites of cyclophosphamide.

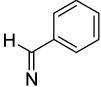
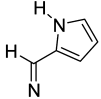
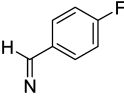
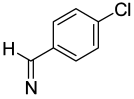
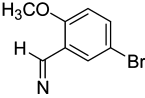
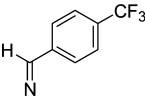
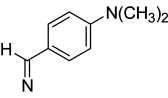
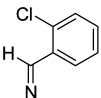
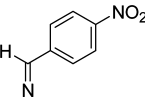
Several synthetic drugs and prodrugs exhibiting inhibition potency against GSTs have been proposed as strategies to overcoming multiple drug resistance (MDR) attributed to GST overexpression.^{11,12} Ethacrynic acid was one of the first inhibitors to be utilized to sensitize cancer cells to the cytotoxic effect of several chemotherapeutic drugs.¹³ Its analogues,^{14–16} individual compounds,^{11,17} and several prodrug molecules^{18–21} have been proposed as GST-inhibiting strategies. Furthermore, several GSH analogues have been proposed as more specific reversible^{22–24} and irreversible²⁵ GST inhibitors, exploiting the high affinity of GSTs for the tripeptide substrate GSH. An alternative concept exploits the susceptibility of GSH

Received: April 5, 2012

Table 1. Structures and Some Properties of the New Arylmethylsulfonylpyrrole Derivatives 4–14



Core structure

Compound ^a	R	molecular formula	molecular weight ^b	hGSTA1-1 inhibition ^c (%)	QlogPo/w ^d
5	NH ₂	C ₁₂ H ₁₄ N ₂ O ₂ S	251.0840 (250.32)	28.0	1.711
6		C ₁₉ H ₁₈ N ₂ O ₂ S	339.1157 (338.42)	30.2	3.528
14		C ₁₇ H ₁₇ N ₃ O ₂ S	328.1105 (327.40)	36.0	3.115
11		C ₁₉ H ₁₇ FN ₂ O ₂ S	357.1059 (356.41)	37.1	3.763
4	NO ₂	C ₁₂ H ₁₂ N ₂ O ₄ S	281.0595 (280.30)	44.3	1.601
13		C ₁₉ H ₁₇ ClN ₂ O ₂ S	373.0759 (372.87)	60.4	4.403
10		C ₂₀ H ₁₉ BrN ₂ O ₃ S	447.0363 (447.35)	64.6	4.080
7		C ₂₀ H ₁₇ F ₃ N ₂ O ₂ S	407.1026 (406.42)	68.4	4.897
8		C ₂₁ H ₂₃ N ₃ O ₂ S	382.1575 (381.49)	78.9	4.598
12		C ₁₉ H ₁₇ ClN ₂ O ₂ S	373.0761 (372.87)	88.8	3.814
9		C ₁₉ H ₁₇ N ₃ O ₄ S	384.1010 (383.42)	90.0	2.768

^aAs in Scheme 1 and in ascending order of inhibition potency against hGSTA1-1. ^bFound by high resolution mass spectrometry as [M + H]⁺ (calculated from the molecular formula for experimental use). ^cMean value of at least three enzyme activity assays (0.1 mM pyrrole derivative); error up to 3%. ^dPredicted octanol/water partition coefficient.

conjugates (products of GST catalysis) against the GSH-degrading enzyme γ -glutamyltranspeptidase (γ GT). Accordingly, certain peptidase-stable GSH analogues have been put to the test as GST inhibitors.^{26–29}

Pyrroles have not been studied so far as GST inhibitors, although sulfonylpyrrole derivatives (Figure SI-1 in Supporting Information) that are part of carbocyclic–SO₂–carbocyclic, carbocyclic–SO₂–heterocyclic, or aliphatic–SO₂–heterocyclic moieties have been found to exhibit a variety of important biological activities. For example, 2-nitrophenylphenylsulfone (Figure SI-1, 6, NPPS),³⁰ 5-chloro-3-(phenylsulfonyl)indole-2-

carboxamide (Figure SI-1, 7, L-737,126),³¹ and ethyl 1-[(2-amino-5-chlorophenyl)sulfonyl]-4-(hydroxymethyl)-1H-pyrrole-2-carboxylate (Figure SI-1, 8, PAS)^{32,33} were lead compounds selected as potent inhibitors of the reverse transcriptase (RT). RT is a virus-encoded enzyme that catalyzes the transcription of single-stranded viral genomic RNA into double-stranded DNA, which is an essential component of the life cycle of HIV-1 (human immunodeficiency virus) responsible for the manifestation of AIDS. Further study of these non-nucleoside reverse transcriptase inhibitors (NNRTIs) showed that ethyl 1-[(5-amino-2-chlorophenyl)sulfonyl]-4-

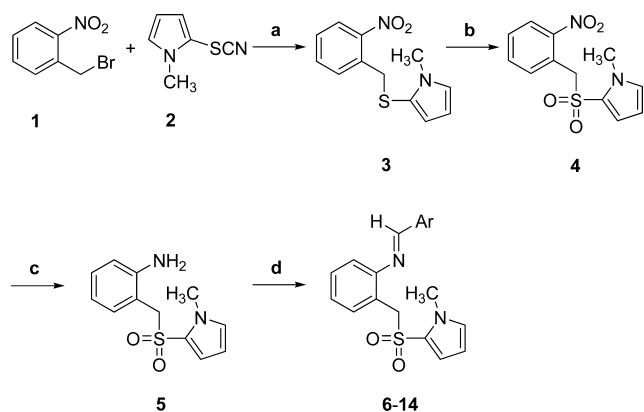
(hydroxymethyl)-1*H*-pyrrole-2-carboxylate (Figure SI-1, **9**)³⁴ is more active than (Figure SI-1, **8**) and that several *N*⁵-benzyl-*N*⁵-methyl-3-(phenylsulfonyl)-1*H*-pyrrole-2,5-dicarboxamide derivatives **10** (Figure SI-1) have been patented as RT inhibitors,³⁵ whereas {4-[(4,5-dihydro-1,3-thiazol-2-ylmethyl)sulfonyl]-1*H*-pyrrol-3-yl}(phenyl)methanones **11** and **12** (Figure SI-1) showed excellent activity against Gram-positive bacteria and good activity against Gram-negative bacteria.³⁶

Herein we report on the synthesis of 11 pyrrole derivatives **4–14** and their inhibitory profile toward hGSTA1-1. Specifically, the 2-(pyrrolesulfonylmethyl)-*N*-arylimine structure was investigated as an inhibitory pharmacophore against hGSTA1-1. Following GST inhibition screening, in silico molecular docking, and enzyme inhibition kinetics, the pyrrole analogue identified as exhibiting the highest inhibitory potency and structural redesign flexibility would be regarded as a new “lead compound” useful in constructing new inhibitors and respective prodrugs for human GSTs of medical importance.

CHEMISTRY

Compounds **4–14** (Table 1) were synthesized according to the route depicted in Scheme 1. In the first step 1-(bromomethyl)-

Scheme 1. Synthetic Route Leading to Arylmethylsulfonylpyrrole Derivatives 4–14^a



^aReagents and conditions: (a) (1) NaBH₄, dry *i*-PrOH, 0 °C, 1.5 h; (2) 1 M NaOH in H₂O, 0 °C to room temp, 2 h; (b) 2KHSO₅·KHSO₄·K₂SO₄, H₂O, MeOH, room temp, 14 h; (c) FeSO₄·7H₂O, 25% NH₄OH, EtOH, 2 h; (d) ArCHO, dry *i*-PrOH, glacial CH₃CO₂H, Na₂SO₄, argon, under reflux, 10 h.

2-nitrobenzene (**1**) was obtained by heating 2-nitrotoluene with NBS and a catalytic amount of benzoyl peroxide in carbon tetrachloride according to Kalir.³⁷ Thiocyanation of 1-methyl-1*H*-pyrrole to 1-methyl-1*H*-pyrrol-2-yl thiocyanate (**2**) took place using ammonium thiocyanate in the presence of molecular iodine in methanol following the procedure of Yadav et al.³⁸ It was found that an optimum yield of 63% was obtained for 1-methyl-2-[(2-nitrobenzyl)sulfonyl]-1*H*-pyrrole (**3**) by reacting bromide **1** with thiocyanate **2** and sodium borohydride in dry ethanol under argon at 0 °C and then allowing the reaction mixture to reach room temperature. Compound **3** is unstable but can be stored for several weeks at ≤0 °C. In the next step, sulfonylpyrrole **3** was dissolved in methanol and oxidized by the dropwise addition of 2 equiv of peroxymonosulfuric acid in water to give 1-methyl-2-[(2-nitrobenzyl)sulfonyl]-1*H*-pyrrole (**4**) in 68% yield. Reduction of the nitro group of **4** took place in ethanol using ferrous

sulfate heptahydrate and 25% ammonium hydroxide at reflux temperature to afford 2-[(1-methyl-1*H*-pyrrol-2-ylsulfonyl)methyl]aniline (**5**) in 88% yield. In the last step aniline **5** was condensed with benzaldehyde, 4-trifluoromethylbenzaldehyde, 4-dimethylaminobenzaldehyde, 4-nitrobenzaldehyde, 5-bromo-2-methoxybenzaldehyde, 4-fluorobenzaldehyde, 2-chlorobenzaldehyde, 4-chlorobenzaldehyde, or 1*H*-pyrrole-2-carbaldehyde by heating in dry propan-2-ol under argon containing dry sodium sulfate and a few drops of glacial acetic acid. The corresponding imines **6–14** were obtained in yields of 40–87%. In the ¹H NMR spectra of imines **6–14** characteristic features are the singlet in the region 4.66–4.73 ppm, integrating for two protons corresponding to the methylene group and the singlet in the region 7.68–8.32 ppm and integrating for one proton corresponding to the imine proton.

RESULTS AND DISCUSSION

Arylmethylsulfonylpyrrole Derivatives Screening and in Silico Study with hGSTA1-1. In order to reveal the inhibitory potency of the arylmethylsulfonylpyrroles against hGSTA1-1, all compounds were subjected to experimental screening against hGSTA1-1 activity, aided by in silico molecular docking. It is evident (Table 1) that all compounds sharing the arylmethylsulfonylpyrrole core structure inhibit hGSTA1-1 activity to a different extent. Figure 1a is an in silico presentation of the V-shaped binding area of hGSTA1-1 derived from crystallographic data of the isoenzyme structure as a complex with the substrates ethacrynic acid and glutathione (PDB code 1GSE). The V-shaped binding area consists of a catalytic primary site (Figure 1a, upper area), designated as the H-site, where hydrophobic substrates bind (CDNB, ethacrynic acid, etc.), and of a neighboring secondary site (Figure 1a, bottom area) where the same and other ligands may bind as well. The hydrophilic tripeptide substrate GSH binds at the G-site located in front of the entrances leading to the V-shaped binding sites (Figure 1a, left area). In agreement with the catalytic function of the enzyme, the present model predicts proximity between the OH group of the catalytically essential Tyr9 residue, the Cl atom of CDNB, and the sulfhydryl group of GSH (Figure 1a and Figure SI-2). Furthermore, two orthogonal views of space-filling models of the arylmethylsulfonylpyrrole (shown in analogue **9**, Figure SI-3) confirm the advantage of choosing this core structure in terms of analogue complementarity with the GST binding site and the shape compliance with the V-shaped binding pocket. In more detail, Figure 1b presents the optimal view of interaction of the core structure present on derivative **9** as follows, going clockwise: (A) the methylated pyrrole fits tightly in the hydrophobic pocket formed by residues Ala12, the hydrophobic part of the side chain of Lys205, Pro206, Pro207, and Met208; (B) the sulfone interacts with the guanidine group of Arg13 and is exposed to solvent; (C) the aryl ring is tightly packed between hydrophobic Leu109, Pro110, and Tyr166; (D) a terminal *p*-nitroarylimine moiety is shown (present on analogue **9**), located in the exit polar/charged channel facing the terminal carboxylate of the substrate GSH.

On the basis of the enzyme inhibition screening of the pyrrole derivatives (Table 1), one distinguishes three groups of inhibitory potency: a group of low inhibition (up to approximately 30%, compounds **5** and **6**), a group of medium inhibition (approximately 35–70%, compounds **14**, **11**, **4**, **13**, **10**, and **7**), and a group of high inhibition (above approximately 80%, compounds **8**, **12**, and **9**). In addition, bromosulpho-

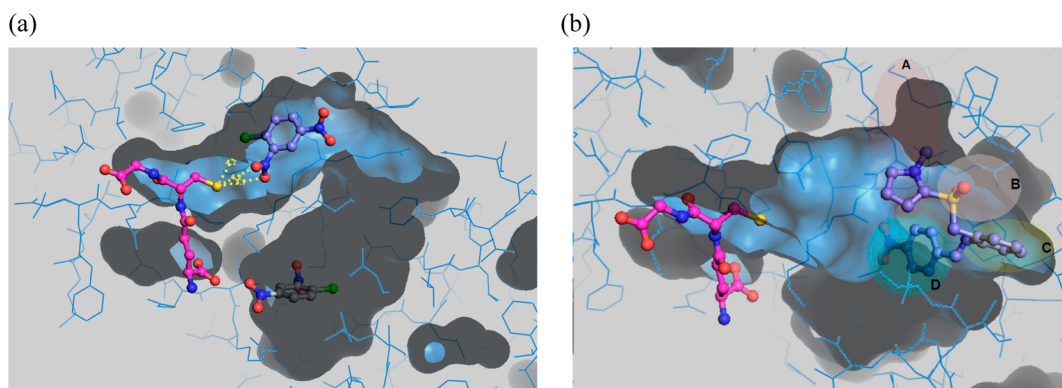


Figure 1. Low energy conformations of the substrates CDNB and GSH with (a) the arylmethylsulfonylpyrrole core structure present on inhibitor **9** (b) at the binding sites of hGSTA1-1 as predicted by *in silico* molecular docking. All ligands are shown as ball-and-stick renditions. GSH is depicted in magenta. Cl atoms are in green, S atoms in yellow, N atoms in blue, and O atoms in red. The figure is created using the PYMOL program, version 1.4. (a) CDNB is bound in two locations of the enzyme V-shaped binding area (gray shade): the catalytic primary (upper area; CDNB is depicted in violet), bound in the catalytically favored orientation having the departing Cl atom opposite the reactive SH-group of GSH and the secondary (lower area) binding sites. (b) Binding mode of the arylmethylsulfonylpyrrole core structure of compound **9** is the following, going clockwise: (A) the CH₃-pyrrole fits in the hydrophobic pocket formed by residues Ala12, the hydrophobic part of the side chain of Lys205, Pro206, Pro207, and Met208; (B) the sulfone interacts with the guanidine group of Arg13 and is exposed to solvent; (C) the aromatic ring is tightly packed between hydrophobic Leu109, Pro110, and Tyr166; (D) the *p*-nitroarylimino moiety, present on inhibitor **9**, is located in the exit polar/charged channel toward the terminal carboxylate of GSH.

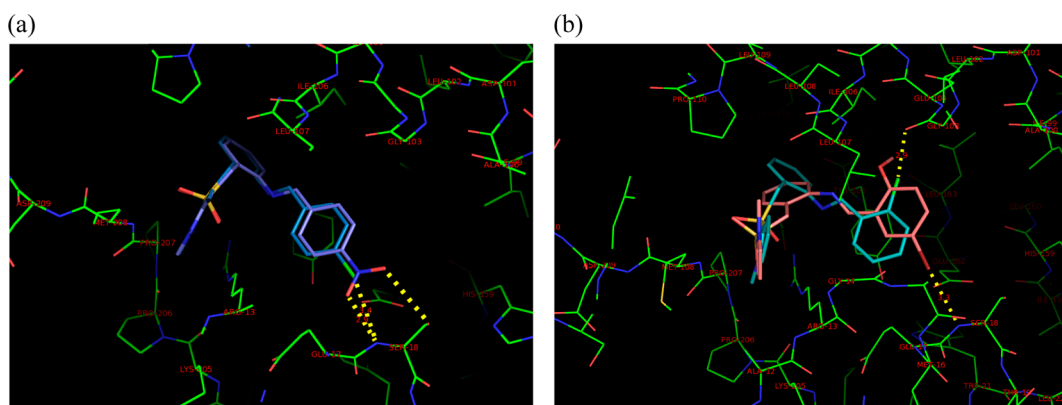


Figure 2. Inhibitors **9** and **13** (a) and inhibitors **10** and **12** (b) in the binding sites of hGSTA1-1. Inhibitors occupy parts of the primary (left area) and secondary (right area) binding sites of the enzyme. (a) Interactions of inhibitors **9** (violet) and **13** (blue). The subsite A (part of the secondary binding site) is located toward the bottom area where hydrogen- and halogen-bond interactions are formed with inhibitors **9** and **13**, respectively. The O atoms (in red) of the *p*-nitro group of inhibitor **9** form H-bond interactions with the backbone HN group (in blue) (2.9 Å) and the HO group (in red) (3.3 Å) of Ser18. The *p*-Cl atom (in green) of inhibitor **13** interacts with the backbone nitrogen atom (in blue) (3.3 Å) of Ser18. (b) Interactions of inhibitors **10** (pink) and **12** (turquoise). The subsite B (part of the secondary binding site) is located toward the upper area where a halogen-bond interaction may be formed between the *o*-Cl atom (in green) of inhibitor **12** with the backbone O atom (in red) (2.9 Å) of Gly103. The *m*-Br atom (in dark red) of inhibitor **10** interacts with the backbone N atom (in blue) (3.3 Å) of Ser18. Interactions are depicted by dotted yellow lines. The figure is created using the PYMOL program, version 1.4.

thalein (BSP) was put in the test as a control inhibitor³⁹ under the same conditions as for the pyrrole derivatives and found to inhibit hGSTA1-1 by approximately 63%. All but two small analogues (**4** and **5**, lacking the arylimino moiety) bind uniquely at the V-shaped deep binding site of hGSTA1-1 (Figure SI-4). One distinguishes substituents of varying chemical nature and position. The *para*-substituted derivative **9** is comparatively the most potent inhibitor (90.0%, Table 1), followed by the *ortho*-substituted derivative **12**. The electronegative *p*-nitro group of the nitrophenylimino moiety creates H-bond interactions with the protein's donor groups in subsite A formed around residues 13–18 (Figure 2a), compared with the *p*-chlorine atom of analogue **13** (60.4%) (Figure 2a) or the *p*-fluorine atom of analogue **11** (37.1% inhibition) forming a weak single halogen interaction (also termed “halogen bond”,

partial charge electrostatic interaction)^{40,41} with the backbone nitrogen atom (in blue) of Ser18. Analogue **13** is a stronger inhibitor compared to **11** probably because of its elevated hydrophobic character, as evidenced by its higher prediction octanol/water partition coefficient QPlogPo/w (Table 1, 4.4 for inhibitor **13** and 3.8 for inhibitor **11**), which generally ranges from –2 for the most polar compounds to 6.5 for the most hydrophobic ones.^{42,43} Although the two other *para*-substituted derivatives (**7** and **8**) fail to develop strong hydrogen bonds, they still show good inhibitory potency (68.4% and 78.9%, respectively), probably due to their high hydrophobic character (QPlogPo/w equals 4.9 for compound **7** and 4.6 for compound **8**) favoring binding to GSTs.

Inhibitor **12** with the Cl atom in the *ortho* position and inhibitor **10** with the Br atom in the *meta* position interact with

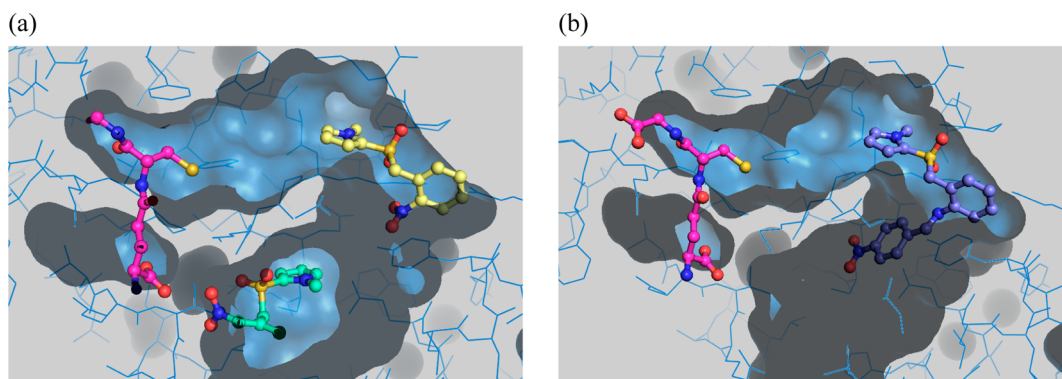


Figure 3. Low energy conformations of substrate GSH and inhibitors **4** (a) and **9** (b) at the most probable binding sites of hGSTA1-1 as predicted by *in silico* molecular docking. All ligands are shown as ball-and-stick renditions. The figure is created using the PYMOL program, version 1.4. (a) Inhibitor **4** is bound in the catalytic primary (yellow ligand) and the noncatalytic secondary (turquoise ligand) binding sites. (b) Inhibitor **9** occupies parts of the catalytic primary (upper area) and secondary (bottom area) binding sites. GSH is depicted in magenta, and the S atom is in yellow. N atoms are in blue and O atoms in red.

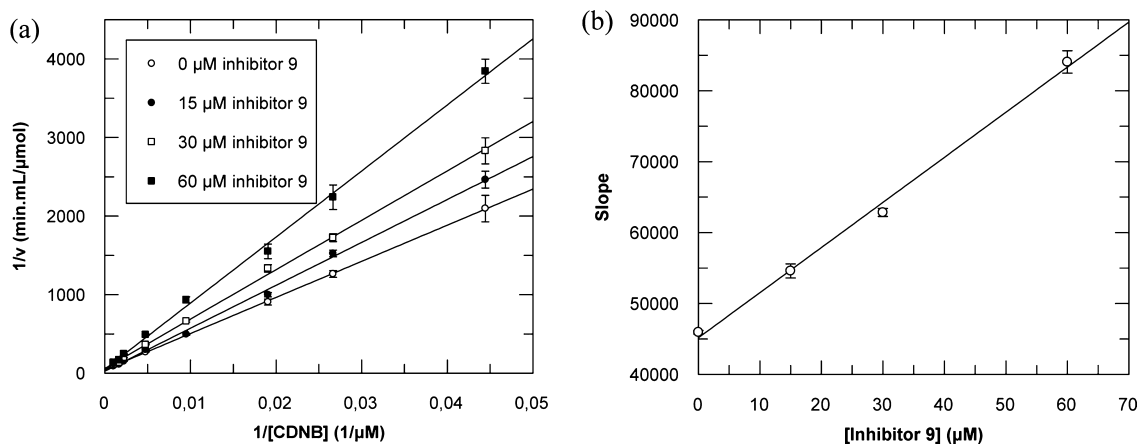


Figure 4. Purely competitive inhibition kinetics of hGSTA1-1 with inhibitor **9** using CDNB as a variable substrate. (a) Lineweaver–Burk (double reciprocal) plot of initial velocities of hGSTA1-1 vs [CDNB] (22.5–990 μM) at different concentrations of inhibitor **9** (0–60 μM). (b) Secondary plot derived from data of plot (a). The inhibition constant K_i for inhibitor **9** is the intercept on the basis axis of plot (b). Points are the average of three enzyme assays. The plot is created using the GraFit program, version 3.

the protein backbone, the former (**12**) forming a halogen-bond interaction with the more electronegative backbone O of Gly 103 in subsite B and the latter (**10**) forming an interaction with the backbone nitrogen atom of Ser 18 in subsite A (Figure 2b). This feature, when combined with a good hydrophobic character (QPlogPo/w equals 3.8 for compound **12** and 4.1 for compound **10**), leads to fairly effective inhibition.

Compound **6**, possessing no polar group on the aromatic ring, expectedly shows much smaller inhibition. Furthermore, the two shorter derivatives (**4** and **5**) lack the arylimino moiety and differ only by the substituent of the aromatic group: a nitro group for **4** and an amino group for **5**, the latter being the “parent” compound from which all others were synthesized (Scheme 1). Compound **4** possessing a nitro group but without the nitrophenylimino moiety binds in the most probable position of binding (catalytic primary binding site) for all arylimino-bearing analogues and with higher flexibility but without formation of apparent H-bond interactions (Figure 3a, yellow ligand), while a second probable binding position toward the protein surface (part of the secondary binding site) and closer to the entrance leading to the deep binding area is predicted (Figure 3a, turquoise ligand), allowing the formation of H-bond interactions with the protein (not shown).

On the basis of the experimental findings and *in silico* interpretations, the arylmethylsulfonylpyrrole core structure can be regarded as a new pharmacophore for hGSTA1-1. Compound **9** (the most potent arylimino-bearing inhibitor) and compound **4** (the most potent small inhibitor), both sharing a terminal *p*-nitro group and the arylmethylsulfonylpyrrole core structure, were chosen for further investigation by enzyme inhibition kinetics in order to better understand their interaction with hGSTA1-1.

Kinetic Inhibition Studies of hGSTA1-1 with the Arylmethylsulfonylpyrroles **4 and **9**.** Prior to proceeding with the kinetic inhibition experiments, control studies were implemented with our enzyme preparation using BSP as a known hGSTA1-1 inhibitor.³⁹ *In silico* molecular docking analysis predicted interaction of BSP with a noncatalytic binding site of hGSTA1-1, allowing binding of CDNB in the catalytic primary site (Figure SI-5a). In agreement with earlier observations,³⁹ this result was confirmed by kinetic inhibition studies using BSP and CDNB as a variable substrate showing a noncompetitive mode of inhibition for hGSTA1-1 (Figure SI-5b). Under the same experimental conditions, benzylsulfonyl-GSH has shown a competitive mode of inhibition.¹⁹

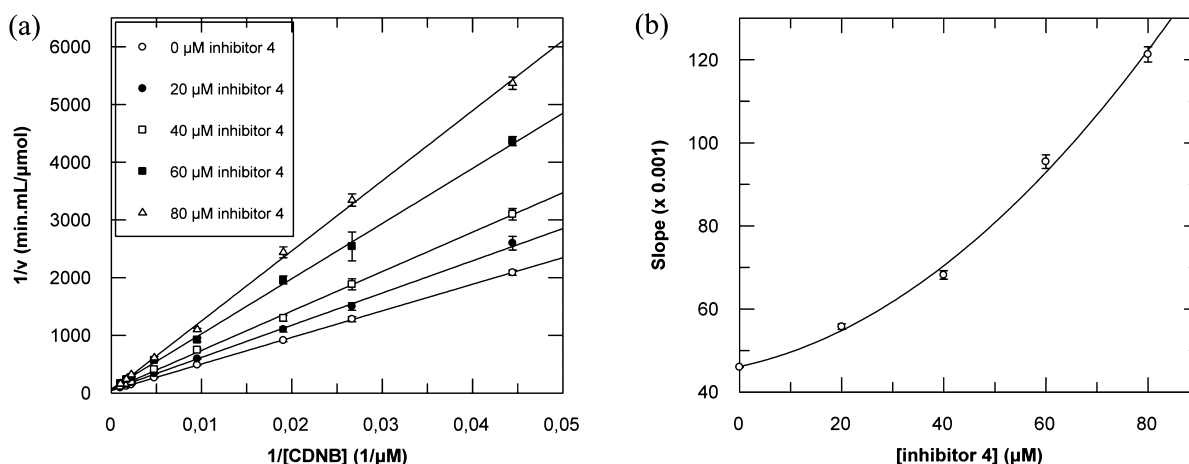


Figure 5. Parabolic competitive inhibition kinetics of hGSTA1-1 with inhibitor 4 using CDNB as a variable substrate. (a) Lineweaver–Burk (double reciprocal) plot of initial velocities of hGSTA1-1 against [CDNB] (22.5–990 μM) at different concentrations of inhibitor 4 (0–80 μM). (b) Secondary plot derived from data of plot (a). Points are the average of three enzyme assays. The plot is created using the GraFit program, version 3.

(a) Inhibition Studies of hGSTA1-1 with Compound 9.

Two sets of experiments were accomplished, each using either CDNB (22.5–990 μM) or GSH (40–2475 μM) as a variable substrate, in the presence of compound 9 at different constant concentrations (0, 15, 30, and 60 μM).

With CDNB as a variable substrate, compound 9 displayed a purely competitive inhibition profile on the basis of the linearity observed for both the double reciprocal graph (Figure 4a) and its secondary plot (Figure 4b).^{44–46} This behavior implies that inhibitor 9 competes with CDNB for the same binding site of GST, calculated inhibition constant $K_{i(9)} = 71 \pm 4 \mu\text{M}$ (from Figure 4b).

This kinetic model is supported by *in silico* molecular docking suggesting that inhibitor 9 is large enough so that when bound to GST, it restricts CDNB from binding at the catalytic primary site of the enzyme. Figure 3b shows the V-shaped binding site of the enzyme in complex with inhibitor 9 occupying parts of the catalytic primary and the secondary sites, and the substrate GSH at its G binding site (left) located in front of the entrances leading to the V-shaped binding sites.

With GSH as a variable substrate, compound 9 has shown a mixed inhibition profile, being evident from the lines of the primary double reciprocal plot of initial velocities of hGSTA1-1 vs [GSH] intersecting to the left of the reciprocal velocity axis (Figure SI-6).^{44,45} Furthermore, the linearity observed with the secondary plots depicting slope or intercept vs [inhibitor 9] (Figure SI-7) is supportive of a purely mixed type of inhibition.⁴⁵ The equilibrium scheme for this type of inhibition^{45,46} predicts that inhibitor 9 could bind both the free GST (forming GST–9) and the GST–GSH complex (forming GST–GSH–9). The latter case suggests interaction of 9 with a site different from the GSH-binding site, that site being partly the catalytic primary CDNB-binding site, as shown earlier (Figures 3b and 4). In such a case, interaction of the cosubstrate CDNB with either of complexes GST–9 and GST–GSH–9 is restricted because of competition between CDNB and inhibitor 9 for the same site; hence both GST–9 and GST–GSH–9 are dead-end (unreactive) complexes. Conclusively, the large inhibitor 9, bearing the arylimino moiety, binds at the V-shaped binding site in a manner prohibiting simultaneous CDNB and GSH binding for catalytic function, rendering impossible the formation of catalytic quadruple complex, i.e., simultaneous binding of CDNB,

GSH, and inhibitor 9 on the same hGSTA1-1 molecule. Nonetheless, this possibility exists for the small inhibitor 4 (section b).

(b) Inhibition Studies of hGSTA1-1 with Compound 4.

Two sets of experiments were accomplished, each having either CDNB (22.5–990 μM) or GSH (40–2475 μM) as a variable substrate, in the presence of inhibitor 4 at different constant concentrations (0, 10, 20, 40, 60, and 80 μM).

With CDNB as a variable substrate, for inhibitor 4 lacking the arylimino moiety the criterion for competitive inhibition is satisfied only on the basis of the observed linearity and the common intercept on the vertical axis for the double reciprocal graph of initial velocities of hGSTA1-1 vs [CDNB] at various constant concentrations of inhibitor 4 (Figure 5a). However, the derived secondary plot (Figure 5b) reveals a parabolic competitive inhibition profile (S-linear I-parabolic competitive inhibition) with the points of the plot curving upward.^{44,46} Therefore, it is conceivable that the binding of small molecule 4 at the large V-shaped binding site of GST would not stop or restrict the binding of a second molecule of inhibitor 4 so that two molecules of 4 could be bound to GST. This kinetic model is confirmed by *in silico* molecular docking, predicting the catalytic primary and noncatalytic secondary binding sites as the two most probable locations for binding to occur (Figure 3a). This view is strengthened by earlier observations suggesting the existence of multiple binding sites with GSTs for a single compound, often with different affinity and inhibitory activity.^{12,39,47–49} For example, isothermal titration calorimetry and kinetic studies of hGSTA1-1 with BSP indicated that each subunit possesses two types of binding sites for BSP, one of which is located at or near the active site and is capable of binding BSP in a noncompetitive manner versus CDNB.^{39,48} Since BSP and CDNB bind to different sites in hGSTA1-1 (Figure SI-5), it is conceivable that the inhibition caused by BSP could be attributed to structural changes resulting in reduced binding/catalytic ability of the substrate by the active site.^{47,48} Therefore, it is reasonable to assume that binding of inhibitor 4 to the noncatalytic secondary site of GST could affect the catalytic function of the adjacent primary binding site, leading to a further decline of activity and increase of inhibition in addition to that occurring upon binding of 4 to the catalytic site alone (Figure 2a). This is in agreement with crystallographic observations⁵⁰ according to which ligand binding is

sensitive to conformational changes in the C-terminal region of hGST A1-1 and this region forms part of the active site. The different conformations of the C-terminal region suggest that structural cooperativity could play a role in the activity of the enzyme.^{48–50} The nonlinearity observed by the secondary plot (Figure 5b) leads to calculating the inhibition constant for analogue **4** from a linear double reciprocal plot, exploiting the Δ slope function against concentration of inhibitor **4** ($K_{i(4)} = 135 \pm 27 \mu\text{M}$) (Figure SI-8).⁴⁵ A comparison of the inhibition constants of compounds **4** and **9** leads to the conclusion that compound **9** may serve as a lead structure for further exploitation. This is supported by the substantially lower free energy of binding (FEB, *in silico* calculations) for compound **9** (-9.82 kcal/mol) compared to compound **4** (-7.33 kcal/mol).

With GSH as a variable substrate, compound **4** has shown a partially mixed inhibition profile (equivalent to S-linear I-hyperbolic noncompetitive inhibition),⁴⁶ as indicated by the lines of the primary double reciprocal graph of initial velocities of hGSTA1-1 vs [GSH] intersecting the left of the reciprocal velocity axis (Figure SI-9) and the nonlinear pattern of the derived secondary plot that curves downward to a limiting rate (Figure 6). These findings are supportive of an inhibition

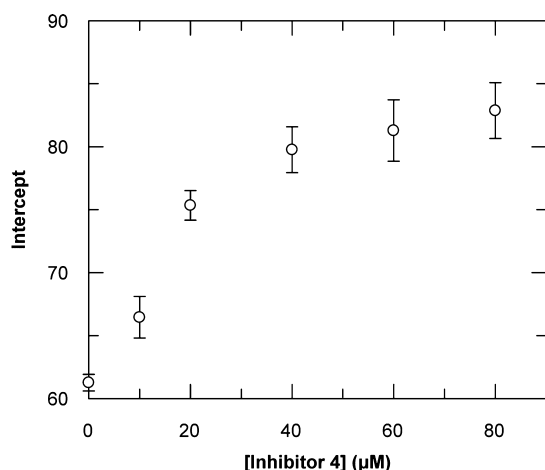


Figure 6. Secondary plot showing the partially mixed inhibition kinetics of hGSTA1-1 with inhibitor **4** using GSH as a variable substrate. The plot is derived from data of the Lineweaver–Burk plot depicting initial velocities of hGSTA1-1 vs [GSH] at different inhibitor concentrations (shown in Figure SI-9). The plot is created using the GraFit program, version 3.

model^{45,46} predicting the small inhibitor **4** to bind at the free GST and the GST–GSH complex, leading to formation of at least two complexes, GST–CDNB–**4** and GST–CDNB–GSH–**4**, respectively, with a CDNB molecule possibly present on the complexes because of use of enzyme-saturating CDNB concentration in the respective assays. Although the GST–CDNB–**4** complex is unreactive, this model foresees breakdown of the GST–CDNB–GSH–**4** complex to products at a rate less than that in the absence of inhibitor.^{45,46} This could be possible if one assumes that inhibitor **4** binds at sites different from the GSH- and CDNB-binding sites, predicting simultaneous binding of three molecules (inhibitor **4** and the two substrates) on the same GST molecule for catalytic function to occur. This model is in agreement with *in silico* molecular docking, predicting a primary and a secondary location in the V-shaped binding site of hGSTA1-1 as the two most probable binding locations for CDNB (Figure 1a). When the nonreactive

secondary site is being occupied by inhibitor **4** rather than a CDNB molecule, a reactive quadruple complex is formed (Figure 7) as a result of simultaneous binding of CDNB, GSH,

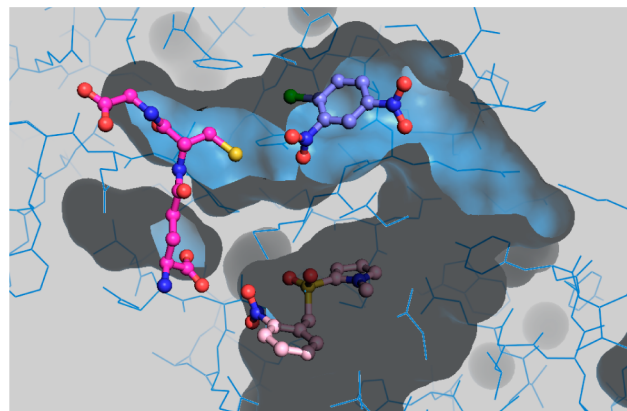


Figure 7. Quadruple catalytic complex of hGSTA1-1 with CDNB, GSH, and inhibitor **4** as predicted by *in silico* molecular docking. All ligands are shown as ball-and-stick renditions. CDNB (in violet) is bound in the catalytic primary site, whereas inhibitor **4** (in pink) is bound in the noncatalytic secondary site. GSH is depicted in magenta, Cl atom in green, and S atom in yellow. N atoms are in blue and O atoms in red. The figure is created using the PYMOL program, version 1.4.

and inhibitor **4** on the same hGSTA1-1 molecule. By combining these findings with those obtained from using CDNB as a variable substrate, one concludes that inhibitor **4** is small enough to interact with the catalytic CDNB-binding site forming a dead-end (unreactive) complex and with the secondary site forming a catalytic (reactive) complex, in the latter case the catalytic site being occupied by CDNB.

CONCLUDING REMARKS

This is the first report on pyrrole inhibitors against GSTs. Eleven new arylmethylsulfonylpyrrole derivatives were synthesized and studied with human GSTA1-1 involved in MDR. *In silico* molecular modeling revealed two locations in the V-shaped binding site where the pyrrole analogues could be accommodated: the primary reactive one in the vicinity of GSH's sulfhydryl group, where both shorter and longer analogues could be accommodated, and the nonreactive secondary one toward the C-terminal of the glutamate of GSH, where smaller analogues can also noncompetitively occupy. Enzyme inhibition screening indicated the arylmethylsulfonylpyrrole core structure as being a new pharmacophore and the 2-(pyrrolesulfonylmethyl)-*N*-4-nitrophenylimine derivative **9** as exhibiting the highest inhibitory potency. Inhibitor **9** competitively binds partly at the catalytic primary site against the substrate CDNB and extends its interaction also with the secondary site, thus prohibiting simultaneous CDNB binding. A smaller inhibitor (**4**) lacking the arylimino moiety can bind at both the primary and secondary sites. The advantage of the present new derivatives, apart from the complementarity with the binding site elements formed by the GST side chains, is the shape compliance with the V-shaped binding pocket. Hence, compound **9** is regarded as a lead structure useful in designing new inhibitors and respective prodrugs against human GSTs.

EXPERIMENTAL SECTION

Chemistry. Melting points were taken on a Büchi 510 apparatus and are uncorrected. Unless otherwise noted, reactions were carried out under an argon atmosphere in a flame-dried, three-neck round-bottomed flask with magnetic stirring. Organic solutions were concentrated by rotary evaporation at 23–40 °C under 15 Torr. ¹H and ¹³C NMR spectra were measured in CDCl₃ or DMSO-*d*₆ on a 250, 400, or 500 MHz Bruker spectrometer. ¹H chemical shifts are reported in ppm from TMS as internal standard, with residual chloroform appearing at 7.26 ppm or DMSO-*d*₆ at 2.50 ppm. ¹³C NMR chemical shifts are reported in ppm from TMS as internal standard, with residual chloroform (77.00 ppm) or DMSO-*d*₆ (39.43 ppm). High resolution ESI mass spectra were measured on a Thermo Fisher Scientific LTQ-ORBITRAP/LC-MS system. Low resolution ESI spectra were measured with an Agilent 1100/LC-MS system. IR spectra were acquired on a Perkin-Elmer 257 or a Perkin-Elmer GX FTIR spectrophotometer as liquids between sodium chloride disks or KBr disks for solids and are reported in wavenumbers (cm⁻¹). Analytical thin layer chromatography was performed with TLC plates (Merck 70–230 mesh silica gel). Visualization was done under a 254 nm UV light source and generally by immersion in acidic aqueous ethanolic vanillin solution or in potassium permanganate (KMnO₄), followed by heating using a heat gun. Purification of reaction products was generally done by dry-column flash chromatography⁵¹ using Merck silica gel 60 and/or flash chromatography⁵² using Carlo Erba Reactifs-SDS silica gel 60. Chemicals and solvents were purchased from Aldrich, Alfa Aesar, or Merck and were of the highest possible purity. The purity of the synthesized compounds was checked in a liquid chromatography–UV diode array system coupled to ion-trap mass spectrometry with electrospray ionization interface (LC/DAD/ESI-MSn) and found to be above 95% (indicative example in the Supporting Information Figure SI-10). All LC-MS experiments were performed on a quadrupole ion-trap mass analyzer (Agilent Technologies, model MSD trap SL) retrofitted to a 1100 binary HPLC system equipped with a degasser, autosampler, diode array detector, and electrospray ionization source (Agilent Technologies, Karlsruhe, Germany). All hardware components were controlled by Agilent Chemstation software. The sample was dissolved in MeOH/0.1% formic acid to the desired concentration. Separation was achieved on a reverse-phase 25 cm × 4.6 mm C8 analytical column at a flow rate of 0.4 mL min, using solvent A (MeOH/formic acid, 99.9:0.1 v/v) and solvent B (water or CH₃CN/formic acid, 99.9:0.1 v/v). The elution was in isocratic mode (85% from solvent A for 20 or 30 min). The UV/vis spectra were recorded in the range of 200–400 nm, and chromatograms were acquired at 254, 280, and 302 nm.

1-Methyl-2-[(2-nitrobenzyl)sulfanyl]-1H-pyrrole (3, Scheme 1). To a stirred solution of 1-(bromomethyl)-2-nitrobenzene **1** (6.05 g, 28 mmol) at 0 °C in dry ethanol (100 mL) under an atmosphere of argon was added sodium borohydride (2.44 g, 64 mmol). A solution of 1-methyl-1H-pyrrol-2-yl thiocyanate **2** (4.14 g, 30 mmol) in dry ethanol (20 mL) was added dropwise over a period of 20 min, and the reaction mixture was left stirring at room temperature for 1.5 h. A solution of sodium hydroxide (2 g, 50 mmol) in water (50 mL) was added, and stirring was continued at room temperature for 2 h. The reaction mixture was poured into water (150 mL), acidified with 1 M HCl to pH 5–6, and extracted with dichloromethane (3 × 65 mL). The combined organic extracts were washed with brine (100 mL), dried (Na₂SO₄), and the solvent was evaporated under reduced pressure. The oily residue was purified by column chromatography using as eluant (dichloromethane/hexane, 1:6) to give the title compound as a caramel oil. Yield, 4.02 g, 58%. *R*_f = 0.13 (dichloromethane/hexane, 1:2). IR (Nujol) *v*_{max} 3115, 2954, 1513, 1346, 859 cm⁻¹. ¹H NMR (CDCl₃) δ 3.37 (s, 3H, CH₃), 4.12 (s, 2H, CH₂), 6.05 (dd, 1H, *J* = 3.6, 2.9 Hz, H-4), 6.16 (dd, 1H, *J* = 3.7, 1.8 Hz, H-3), 6.72 (dd, 1H, *J* = 2.5, 2.0 Hz, H-5), 6.98 (dd, 1H, *J* = 7.1, 1.9 Hz, H-6'), 7.50 (m, 2H, H-4', H-5'), 7.97 (dd, 1H, *J* = 7.1, 2.3 Hz, H-3'). ¹³C NMR (CDCl₃) δ 33.44, 39.67, 108.11, 118.74, 124.98, 125.43, 126.75, 127.96, 132.08, 132.86, 133.89, 148.06. HRMS (ESI, MeOH,

0.1% HCO₂H) *m/z* calculated for C₁₂H₁₃N₂O₂S [M + H]⁺ 249.0692, found 249.0685.

1-Methyl-2-[(2-nitrobenzyl)sulfanyl]-1H-pyrrole (4, Table 1). To a stirred solution of 2-[(2-nitrobenzyl)sulfanyl]-1H-pyrrole **3** (2.4 g, 9.7 mmol) in methanol (120 mL) was added a solution of peroxymonosulfuric acid (5.99 g, 9.7 mmol) in water (150 mL), and the mixture was left stirring at room temperature for 4 h. TLC examination of the reaction mixture verified that the reaction was incomplete, and therefore, a further portion of peroxymonosulfuric acid (5.99 g, 9.7 mmol) in water (150 mL) was added dropwise and stirring at room temperature continued for 6 h. The reaction mixture was quenched with water (300 mL) and extracted with dichloromethane (3 × 100 mL). The combined organic extracts were washed with brine (150 mL), dried (Na₂SO₄), and the solvent was evaporated under reduced pressure. The oily residue was purified by column chromatography (ethyl acetate/hexane, 1:2) to give the title compound (1.84 g, 68%) as a yellow solid (microcrystals from toluene), mp 111–112 °C. *R*_f = 0.2 (ethyl acetate/hexane 1:2). IR (Nujol) *v*_{max} 3119, 2956, 1519, 1354, 1316 cm⁻¹. ¹H NMR (CDCl₃) δ 3.63 (s, 3H, CH₃), 4.94 (s, 2H, CH₂), 6.08 (dd, 1H, *J* = 4.0, 2.6 Hz, H-4), 6.53 (dd, 1H, *J* = 4.0, 1.8 Hz, H-3), 6.79 (t, 1H, *J* = 2.2 Hz, H-5), 7.66–7.45 (m, 3H, H-4', H-5', H-6'), 7.96 (dd, 1H, *J* = 8, 1.4 Hz, H-3'). ¹³C NMR (CDCl₃) δ 35.45, 58.99, 108.62, 120.26, 123.40, 125.21, 125.67, 129.87, 130.44, 133.20, 134.45. HRMS (ESI, MeOH, 0.1% HCO₂H) *m/z* calculated for C₁₂H₁₃N₂O₄S [M + H]⁺ 281.0591, found 281.0595.

2-[(1-Methyl-1H-pyrrol-2-ylsulfanyl)methyl]aniline (5, Table 1). To a stirred solution of 1-methyl-2-[(2-nitrobenzyl)sulfanyl]-1H-pyrrole **4** (2.0 g, 7.13 mmol) in hot 95% ethanol (120 mL) was added a suspension of ferrous sulfate heptahydrate (19.9 g, 71.6 mmol) in water (80 mL) followed by 25% ammonium hydroxide (20 mL). The resulting mixture was heated to reflux for 2 h during which 25% ammonium hydroxide (60 mL) was added dropwise. After cooling, the reaction mixture was passed through a pad of Celite, and then the filter aid was washed with small aliquots of hot ethanol. The organic solvent was evaporated under reduced pressure, and the resulting aqueous suspension was extracted with dichloromethane (3 × 40 mL). The combined organic extracts were washed with brine (40 mL), dried (Na₂SO₄), and the solvent was evaporated under reduced pressure. The residue was purified by column chromatography (ethyl acetate/hexane, 1:2) to give the title compound (1.57 g, 88%) as a pale yellow solid (microcrystals from dichloromethane/hexane), mp 111–113 °C. *R*_f = 0.2 (ethyl acetate/hexane, 1:2). IR (nujol) *v*_{max} 3455, 3377, 3128, 2972, 1290, 1170 cm⁻¹. ¹H NMR (CDCl₃) δ 3.19 (s, 3H, CH₃), 4.11 (br s, 2H, NH₂), 4.35 (s, 2H, CH₂), 6.15 (dd, 1H, *J* = 4, 2.6 Hz, H-4), 6.49 (dd, 1H, *J* = 7.6 Hz, 1.5 Hz, H-3'), 6.60 (dd, 1H, *J* = 7.5, 1.2 Hz, H-5'), 6.61 (t, 1H, *J* = 2.2 Hz, H-5), 6.71 (dd, 1H, *J* = 7.4, 0.8 Hz, H-6'), 6.89 (dd, 1H, *J* = 4.0, 1.8 Hz, H-3), 7.11 (dt, 1H, *J* = 7.9, 1.6 Hz, H-4'). ¹³C NMR (CDCl₃) δ 34.97, 61.24, 108.39, 113.95, 117.38, 119.14, 119.42, 125.29, 129.70, 130.07, 132.38, 146.83. HRMS (ESI, MeOH, 0.1% HCO₂H) *m/z* calculated for C₁₂H₁₅N₂O₂S [M + H]⁺ 251.0849, found 251.0840.

General Procedure for the Synthesis of Imines 6–14 (Table 1). To a warm solution of 2-[(1-methyl-1H-pyrrol-2-ylsulfanyl)methyl]aniline **5** (1 mmol) in propan-2-ol (20 mL) under argon was added a few drops of glacial acetic acid until pH 4–5 was obtained, followed by anhydrous sodium sulfate (0.5 g) and benzaldehyde, 4-trifluoromethylbenzaldehyde, 4-dimethylaminobenzaldehyde, 4-nitrobenzaldehyde, 5-bromo-2-methoxybenzaldehyde, 4-fluorobenzaldehyde, 2-chlorobenzaldehyde, 4-chlorobenzaldehyde, or 1H-pyrrole-2-carbaldehyde (1.2 mmol). The reaction mixture was heated under reflux for 10 h. Sodium sulfate was filtered off and the solvent evaporated under reduced pressure. To the residue was added dichloromethane (20 mL). The resulting solution was washed with 20% aqueous sodium bisulfite (3 × 5 mL), brine (10 mL), dried (Na₂SO₄) and the solvent evaporated under reduced pressure to give a solid. The solid was purified by column chromatography (ethyl acetate/hexane, 1:4) to afford imine **6**, **7**, **12**, or **14** or by crystallization to afford imine **8**, **9**, **10**, or **11**.

2-[[[(1-Methyl-1H-pyrrol-2-yl)sulfonyl]methyl]-N-[(1E)-phenyl]methylene]aniline (6, Table 1). Light brown viscous oil (0.20 g, 59%) (column chromatography). $R_f = 0.43$ (ethyl acetate/dichloromethane, 2:1). IR (Nujol) ν_{\max} 3065, 2986 1628, 1313, 1109 cm^{-1} . $^1\text{H NMR}$ (CDCl_3) δ 3.25 (s, 3H, CH_3), 4.73 (s, 2H, CH_2), 5.83 (t, 1H, $J = 2.5$ Hz, H-4), 6.31–6.38 (m, 2H, H-3, H-5), 6.87 (d, 1H, $J = 7.5$ Hz, H-3'), 7.23–7.49 (m, 6H, H-4', H-6', H-5', H-3'', H-4'', H-5''), 7.70–7.79 (m, 2H, H-2'', H-6''), 7.89 (s, 1H, N=CH). $^{13}\text{C NMR}$ (CDCl_3) δ 35.53, 59.17, 108.09, 117.99, 120.02, 123.45, 126.31, 126.32, 128.78, 129.06, 129.75, 130.25, 131.71, 132.44, 135.93, 151.19, 158.01, 159.54. HRMS (ESI, MeOH) m/z calculated for $\text{C}_{19}\text{H}_{19}\text{N}_2\text{O}_2\text{S}$ $[\text{M} + \text{H}]^+$ 339.1162, found 339.1157.

2-[[[(1-Methyl-1H-pyrrol-2-yl)sulfonyl]methyl]-N-[(1E)-[4-(trifluoromethyl)phenyl]methylene]aniline (7, Table 1). Light yellow microcrystals (0.27 g, 67%) (column chromatography, crystallization from dichloromethane/hexane), mp 140–141 °C. $R_f = 0.43$ (ethyl acetate/hexane, 1:2). IR (Nujol) ν_{\max} 3058, 2975, 1632, 1306, 1108, 1326 cm^{-1} . $^1\text{H NMR}$ (CDCl_3) δ 3.17 (s, 3H, CH_3), 4.71 (s, 2H, CH_2), 5.80 (dd, 1H, $J = 3.9, 2.6$ Hz, H-4), 6.36–6.37 (m, 1H, H-5), 6.41 (dd, 1H, $J = 4.0, 1.8$ Hz, H-3), 6.91 (d, 1H, $J = 7.8$ Hz, H-3'), 7.26 (ddd, 1H, $J = 7.4, 1.0$ Hz, H-5'), 7.38 (ddd, 1H, $J = 7.5, 1.4$ Hz, H-4'), 7.45 (dd, 1H, $J = 7.4, 1.2$ Hz, H-6'), 7.70 (d, 2H, $J = 8.17$ Hz, H-2'', H-6''), 7.88 (d, 2H, $J = 8.07$ Hz, H-3'', H-5''), 7.99 (s, 1H, N=CH). $^{13}\text{C NMR}$ (CDCl_3) δ 35.11 (CH_3), 59.15 (CH_2), 108.06 (C-4), 117.67 (C-3'), 119.60 (C-3), 123.41 (C-2'), 125.08 (C-2), 125.43 (C-2'' or C-6''), 125.48 (C-2'' or C-6''), 126.64 (C-5'), 128.94 (C-3'', C-5''), 129.43 (C-5), 130.12 (C-4'), 132.35 (C-6'), 132.42 (C-4''), 132.90 (CF_3), 138.77 (C-1''), 150.31 (C-1'), 157.55 (C=N). HRMS (ESI, MeOH, 0.1% HCO_2H) m/z calculated for $\text{C}_{20}\text{H}_{18}\text{F}_3\text{N}_2\text{O}_2\text{S}$ $[\text{M} + \text{H}]^+$ 407.1036, found 407.1026.

N-[(1E)-[4-(Dimethylamino)phenyl]methylene]-2-[[[(1-methyl-1H-pyrrol-2-yl)sulfonyl]methyl]aniline (8, Table 1). Pale yellow microcrystals (0.23 g, 60%) (crystallization from dichloromethane/hexane), mp 152–154 °C. $R_f = 0.23$ (ethyl acetate/hexane, 1:2). IR (Nujol) ν_{\max} 3119, 2861, 2808, 1588, 1310, 1106 cm^{-1} . $^1\text{H NMR}$ (CDCl_3) δ 3.08 [s, 6H, (CH_3)₂N], 3.30 (s, 3H, CH_3), 4.73 (s, 2H, CH_2), 5.84 (dd, 1H, $J = 3.9, 2.6$ Hz, H-4), 6.32–6.36 (m, 2H, H-5, H-3), 6.71 (d, 2H, $J = 8.9$ Hz, H-3'', H-5''), 6.81 (d, 1H, $J = 7.7$ Hz, H-3'), 7.18 (ddd, 1H, $J = 7.5, 1.1$ Hz, H-5'), 7.31 (ddd, 1H, $J = 7.6, 1.3$ Hz, H-4'), 7.48 (d, 1H, $J = 7.5$ Hz, H-6'), 6.71 (d, 2H, $J = 8.9$ Hz, H-2'', H-6''), 7.68 (s, 1H, N=CH). $^{13}\text{C NMR}$ (CDCl_3) δ 35.49 (CH_3), 40.13 [(CH_3)₂N], 58.85 (CH_2), 107.69 (C-4), 111.27 (C-3'), 118.04 (C-3'), 119.88 (C-3), 122.96 (C-2'), 124.06 (C-1''), 125.01 (C-2), 125.11 (C-5'), 129.56 (C-5), 129.97 (C-4'), 130.61 (C-2'', C-6''), 132.04 (C-6'), 152.04 (C-1'), 152.48 (C-4''), 159.18 (CH=N). HRMS (ESI, MeOH, 0.1% HCO_2H) m/z calculated for $\text{C}_{21}\text{H}_{24}\text{N}_3\text{O}_2\text{S}$ $[\text{M} + \text{H}]^+$ 382.1584, found 382.1575.

2-[[[(1-Methyl-1H-pyrrol-2-yl)sulfonyl]methyl]-N-[(1E)-[4-nitrophenyl]methylene]aniline (9, Table 1). Yellow microcrystals (0.33 g, 87%) (crystallization from ethyl acetate/hexane), mp 173–174 °C. $R_f = 0.32$ (ethyl acetate/hexane, 1:2). IR (Nujol) ν_{\max} 3095, 2988, 1602, 1524, 1346, 1310, 1106 cm^{-1} . $^1\text{H NMR}$ (CDCl_3) δ 3.16 (s, 3H, CH_3), 4.71 (s, 2H, CH_2), 5.80 (dd, 1H, $J = 4.0, 2.6$ Hz, H-4), 6.39 (t, 1H, $J = 2.2$ Hz, H-5), 6.44 (dd, 1H, $J = 4.0, 1.8$ Hz, H-3), 6.94 (d, 1H, $J = 7.2$ Hz, H-3'), 7.30 (ddd, 1H, $J = 7.5, 1.0$ Hz, H-5'), 7.40 (ddd, 1H, $J = 7.6, 1.4$ Hz, H-4'), 7.45 (dd, 1H, $J = 7.6, 1.2$ Hz, H-6'), 7.94 (d, 2H, $J = 8.8$ Hz, H-2'', H-6''), 8.06 (s, 1H, N=CH), 8.30 (d, 2H, $J = 8.8$ Hz, H-3'', H-5''). $^{13}\text{C NMR}$ (CDCl_3) δ 35.21 (CH_3), 60.91 (CH_2), 108.27 (C-4), 117.61 (C-3'), 119.66 (C-3), 123.72 (C-2'), 123.85 (C-3'', C-5''), 125.29 (C-2), 127.18 (C-5'), 129.42 (C-2'', C-6''), C-5), 130.25 (C-4'), 132.60 (C-6'), 141.08 (C-1''), 149.25 (C-4''), 150.07 (C-1'), 156.53 (C=N). HRMS (ESI, MeOH, 0.1% HCO_2H) m/z calculated for $\text{C}_{19}\text{H}_{18}\text{N}_3\text{O}_4\text{S}$ $[\text{M} + \text{H}]^+$ 384.1013, found 384.1010.

N-[(1E)-[5-Bromo-2-methoxyphenyl]methylene]-2-[[[(1-methyl-1H-pyrrol-2-yl)sulfonyl]methyl]aniline (10, Table 1). Pale yellow microcrystals (0.18 g, 40%) (crystallization from dichloromethane/hexane), mp 131–132 °C. $R_f = 0.18$ (ethyl acetate/hexane, 1:2). IR (Nujol) ν_{\max} 3070, 2982, 1622, 1318, 1112, 1268, 1050 cm^{-1} . $^1\text{H NMR}$ (CDCl_3) δ 3.29 (s, 3H, CH_3), 3.89 (s, 3H, OCH_3), 4.71 (s, 2H, CH_2), 5.82 (dd, 1H, $J = 4.0, 2.6$ Hz, H-4), 6.24 (s,

1H, H-3), 6.35 (t, 1H, $J = 1.9$ Hz, H-5), 6.43 (dd, 1H, $J = 4.0, 1.8$ Hz, H-3), 6.83 (d, 1H, $J = 8.8$ Hz, H-3''), 6.90 (d, 1H, $J = 7.1$ Hz, H-3'), 7.25 (ddd, 1H, $J = 7.4, 1.0$ Hz, H-5'), 7.36 (ddd, 1H, $J = 7.5, 1.4$ Hz, H-4'), 7.53–7.46 (m, 2H, H-6', H-4''), 8.07 (d, 1H, $J = 2.5$ Hz, H-6''), 8.32 (s, 1H, N=CH). $^{13}\text{C NMR}$ (CDCl_3) δ 35.38, 55.80, 59.15, 108.01, 113.02, 113.26, 117.97, 119.63, 123.56, 125.01, 126.10, 126.30, 129.42, 129.81, 130.04, 132.43, 135.17, 151.03, 153.49, 158.11. HRMS (ESI, MeOH, 0.1% HCO_2H) m/z calculated for $\text{C}_{20}\text{H}_{20}\text{BrN}_2\text{O}_3\text{S}$ $[\text{M} + \text{H}]^+$ 447.0363, found 447.0363.

N-[(1E)-[4-Fluorophenyl]methylene]-2-[[[(1-methyl-1H-pyrrol-2-yl)sulfonyl]methyl]aniline (11, Table 1). Light brown microcrystals (0.275 g, 78%) (crystallization from methyl *tert*-butyl ether/hexane), mp 93–94 °C. $R_f = 0.27$ (ethyl acetate/hexane, 1:2). IR (Nujol) ν_{\max} 3116, 2922, 1630, 1312, 1110, 1218 cm^{-1} . $^1\text{H NMR}$ (CDCl_3) δ 3.18 (s, 3H, CH_3), 4.69 (s, 2H, CH_2), 5.79 (dd, 1H, $J = 4.0, 2.6$ Hz, H-4), 6.33 (t, 1H, $J = 2.2$ Hz, H-5), 6.38 (dd, 1H, $J = 4.0, 1.9$ Hz, H-3), 6.85 (dd, 1H, $J = 7.8, 1.0$ Hz, H-3'), 7.12 (t, 2H, $J = 8.6$ Hz, H-2'', H-6''), 7.22 (ddd, 1H, $J = 7.6, 1.2$ Hz, H-5'), 7.34 (ddd, 1H, $J = 7.6, 1.5$ Hz, H-4'), 7.44 (dd, 1H, $J = 7.5, 1.4$ Hz, H-6'), 7.75 (dd, 2H, $J = 8.7, 5.5$ Hz, H-3'', H-5''), 7.86 (s, 1H, N=CH). $^{13}\text{C NMR}$ (CDCl_3) δ 35.22 (CH_3), 59.06 (CH_2), 107.96 (C-4), 115.59 (C-3'', C-5''), 115.94 (C-3'', C-5''), 117.78 (C-3'), 119.67 (C-3), 123.15 (C-2''), 125.13 (C-2), 126.13 (C-5'), 129.43 (C-5), 130.08 (C-4'), 130.74 (C-2'', C-6''), 130.88 (C-2'', C-6''), 132.15 (C-1''), 132.25 (C-6'), 150.79 (C-1'), 157.81 (C=N), 164.59 (C-4''). HRMS (ESI, MeOH, 0.1% HCO_2H) m/z calculated for $\text{C}_{19}\text{H}_{18}\text{FN}_2\text{O}_2\text{S}$ $[\text{M} + \text{H}]^+$ 357.1068, found 357.1059.

N-[(1E)-[2-Chlorophenyl]methylene]-2-[[[(1-methyl-1H-pyrrol-2-yl)sulfonyl]methyl]aniline (12, Table 1). Yellow microcrystals (0.28 g, 80%) (column chromatography, crystallization from dichloromethane/hexane), mp 124–125 °C. $R_f = 0.4$ (ethyl acetate/hexane, 1:2). IR (Nujol) ν_{\max} 3123, 2929, 1620, 1308, 1110, 1052 cm^{-1} . $^1\text{H NMR}$ (CDCl_3) δ 3.12 (s, 3H, CH_3), 4.69 (s, 2H, CH_2), 5.76 (t, 1H, $J = 3.2$ Hz, H-4), 6.32–6.33 (m, 2H, H-5, H-3), 6.88 (d, 1H, $J = 7.7$ Hz, H-3'), 7.21–7.37 (m, 5H, H-4', H-5', H-6', H-4'', H-6''), 7.46 (d, 1H, $J = 6.6$ Hz, H-5''), 8.07 (d, 1H, $J = 7.07$ Hz, H-3''), 8.30 (s, 1H, N=CH). $^{13}\text{C NMR}$ (CDCl_3) δ 34.96, 59.09, 107.95, 117.70, 119.37, 123.61, 124.29, 126.37, 126.67, 128.11, 129.38, 129.73, 129.93, 132.19 (2C), 132.21, 135.64, 150.35, 154.83. HRMS (ESI, MeOH, 0.1% HCO_2H) m/z calculated for $\text{C}_{19}\text{H}_{18}\text{ClN}_2\text{O}_2\text{S}$ $[\text{M} + \text{H}]^+$ 373.0772, found 373.0761.

N-[(1E)-[4-Chlorophenyl]methylene]-2-[[[(1-methyl-1H-pyrrol-2-yl)sulfonyl]methyl]aniline (13, Table 1). Colorless microcrystals (0.29 g, 83%) (chloroform/hexane), mp 117–118 °C. $R_f = 0.23$ (ethyl acetate/hexane, 1:2). IR (Nujol) ν_{\max} 3128, 2910, 1626, 1312, 1108, 1088 cm^{-1} . $^1\text{H NMR}$ (CDCl_3) δ 3.16 (s, 3H, CH_3), 4.66 (s, 2H, CH_2), 5.77 (dd, 1H, $J = 3.7, 2.6$ Hz, H-4), 6.29 (s, 1H, H-3), 6.34 (dd, 1H, $J = 3.7, 1.7$ Hz, H-5), 6.82 (d, 1H, $J = 7.7$ Hz, H-3'), 7.24–7.53 (m, 5H, H-4', H-5', H-6', H-2'', H-6''), 7.65 (d, 2H, $J = 8.4$ Hz, H-3'', H-5''), 7.82 (s, 1H, N=CH). $^{13}\text{C NMR}$ (CDCl_3) δ 35.29, 59.09, 108.03, 117.75, 119.75, 123.28, 126.36, 128.93 (2C), 129.46, 129.96 (2C), 130.12, 132.35, 134.20, 137.50, 150.67, 157.80. HRMS (MeOH, 0.1% HCO_2H) m/z calculated for $\text{C}_{19}\text{H}_{18}\text{ClN}_2\text{O}_2\text{S}$ $[\text{M} + \text{H}]^+$ 373.0772, found 373.0759.

2-[[[(1-Methyl-1H-pyrrol-2-yl)sulfonyl]methyl]-N-[(1E)-1H-pyrrol-2-yl]methylene]aniline (14, Table 1). Pale brown microcrystals (0.25 g, 77%) (column chromatography, crystallization from dichloromethane/hexane), mp 134–136 °C. $R_f = 0.21$ (ethyl acetate/hexane, 1:2). IR (Nujol) ν_{\max} 3362, 3119, 2910, 1620, 1296, 1106 cm^{-1} . $^1\text{H NMR}$ (CDCl_3) δ 3.21 (s, 3H, CH_3), 4.69 (s, 2H, CH_2), 5.88 (dd, 1H, $J = 3.9, 2.6$ Hz, H-4), 6.26 (t, 1H, $J = 2.9$ Hz, H-4''), 6.42 (t, 1H, $J = 2.1$ Hz, H-5), 6.46 (dd, 1H, $J = 4.0, 1.8$ Hz, H-3), 6.57 (d, 1H, $J = 2.9$ Hz, H-3''), 6.83 (d, 1H, $J = 7.7$ Hz, H-3'), 6.88 (s, 1H, H-5''), 7.16 (ddd, 1H, $J = 7.4, 0.7$ Hz, H-5'), 7.32 (ddd, 1H, $J = 7.6, 1.3$ Hz, H-4'), 7.40 (dd, 1H, $J = 7.5, 1.0$ Hz, H-6'), 7.68 (s, 1H, N=CH), 9.56 (br, s, 1H, NH). $^{13}\text{C NMR}$ (CDCl_3) δ 34.97 (CH_3), 58.89 (CH_2), 107.65 (C-4), 110.28 (C-4''), 116.33 (C-3''), 117.78 (C-3'), 119.43 (C-3), 122.76 (C-2'), 122.92 (C-5''), 125.12 (C-2), 125.20 (C-4'), 129.66 (C-5), 129.97 (C-5'), 130.46 (C-2''), 132.02 (C-6'), 148.81

(C=N), 151.03 (C-1'). HRMS (MeOH, 0.1% HCO₂H) *m/z* calculated for C₁₇H₁₈N₃O₂S [M + H]⁺ 328.1114, found 328.1105.

Modeling and Docking: In Silico Creation of the hGSTA1-1 Structure and Docking of Pyrrole Analogues to the hGSTA1-1 Model. The structure of glutathione transferase A1-1 (hGSTA1-1) in complex with ethacrynic acid and its glutathione conjugate (PDB code 1GSE) was processed using MGLTools 1.5.4.⁵⁵ The tripeptide substrate glutathione was added to the protein PDBQT file. Docking of the pyrrole analogues to hGSTA1-1 was performed using AutoDock 4.0.⁵⁴ Autodock free-energy scoring function is based on a linear regression analysis, the AMBER force field,⁵⁵ and a large set of diverse protein–ligand complexes with known binding constants. The Lamarckian genetic algorithm (LGA) search method with default parameters was used. Limits for 5 000 000 maximum number of energy evaluations and 50 docking runs were set. All ligands were treated as flexible. Docking results were both visually inspected and quantitatively evaluated based on the estimated free energy of binding (FEB). For identifying the possible binding sites on the protein of the kinetically studied analogues, 4 and 9, the following procedure was used. After docking of the pyrrole analogues, docked analogue 9 was merged in the protein file, the grid maps were recalculated on the resulting complex, and the competing substrate CDNB was docked on it. Similarly, docked analogue 4 was merged with the protein, and CDNB and another 4 molecule were docked on the complex. All figure depicting 3D models were created using PYMOL, version 1.4.⁵⁶

Expression and Purification of hGSTA1-1 from Recombinant *E. coli* cells. This was based on a published method⁵⁷ with modifications. Briefly, *E. coli* BL21 (DE3) cells harboring plasmid pOXO4-GSTA1 were grown in Luria–Bertani (LB) medium containing ampicillin (100 µg/mL) and chloramphenicol (25 µg/mL). The expression of GST was induced by addition of 1 mM isopropyl-β-D-thiogalactopyranoside (IPTG) when the absorbance at 600 nm was 0.6. Four hours after induction, cells (2.5 g) were harvested by centrifugation at 8000 rpm (4 °C) for 20 min and resuspended in 7.5 mL of phosphate buffer (20 mM, pH 7), sonicated (13 × 5 s), and centrifuged at 13 000 rpm for 5 min. A sample of 5 mL from the supernatant (15 mL) was loaded to an affinity chromatography column (2 mL adsorbent) previously equilibrated with potassium phosphate buffer (20 mM, pH 7). The affinity adsorbent (GSH-Sepharose-CL6B) contained the tripeptide glutathione immobilized to cross-linked agarose (Sepharose-CL6B) which was previously epoxy-activated with bis-epoxirane (1,4-butanediol diglycidyl ether) in alkaline solution. Nonadsorbed protein was washed off with 10 mL of equilibration buffer prior to desorbing bound GST in equilibration buffer containing 10 mM GSH (21 mL). Fractions (3 mL each) with enzyme activity were pooled (547 units in 10 mL total), concentrated (3.5 mL, nitrocellulose, cutoff of 10 kDa), diluted by dropwise addition of glycerol to 50% (v/v) final concentration, and stored at –20 °C for several months without appreciable loss of activity (approximately 40 units of GST activity per mL).

Enzyme Assays and Screening of the Arylmethylsulfonylpyrrole Derivatives for hGSTA1-1 Inhibition. *GST Assay.* GST assays were performed by monitoring the formation of the conjugate formed between CDNB and the tripeptide GSH at 340 nm ($\epsilon = 9.6 \mu\text{mol mL}^{-1} \text{cm}^{-1}$) at 25 °C. In a typical volume of 914 µL of potassium phosphate buffer (100 mM, pH 6.5) were added 33 µL of CDNB (30 mM) and 33 µL of GSH (75 mM). DMSO was also added (20 µL, in place of equal volume of buffer) only for inhibition experiments with the arylmethylsulfonylpyrroles. The mixture was incubated at 25 °C for 5 min, prior to adding enzyme sample (typically 20 µL, 0.45 GST unit) in a total assay volume of 1 mL. Initial velocities were determined in triplicate and were corrected for spontaneous reaction rates when necessary. One unit of enzyme activity is defined as the amount of enzyme that produces 1.0 µmol of product per minute at pH 6.5 at 25 °C.

Screening of the Arylmethylsulfonylpyrrole Derivatives as hGSTA1-1 Inhibitors. For enzyme inhibition screening of the arylmethylsulfonylpyrroles (Table 1), the GST assay mixture contained in a total assay volume of 1 mL: potassium phosphate buffer (100 mM, pH 6.5), 33 µL of 30 mM CDNB, 33 µL of 75 mM

GSH, DMSO (concentration in assay of 2%), and pyrrole analogue or the control inhibitor BSP (concentration in assay of 100 µM). The mixture was incubated at 25 °C for 5 min prior to the addition of enzyme (15 µL, 0.5 GST unit). The observed rate was employed for calculating the remaining activity (%), taking as 100% initial activity value the rate observed (up to 0.2 [ΔA/min]₃₄₀) after replacing the arylmethylsulfonylpyrrole by an equal volume of buffer, thus keeping constant the assay total volume (1 mL).

Kinetic Inhibition Studies with hGSTA1-1. Kinetic Analysis of Inhibitors 4 and 9 Using CDNB as a Variable Substrate. Initial velocities for the hGSTA1-1-catalyzed reaction with CDNB as variable substrate were determined in reaction mixtures of a total volume of 1 mL (25 °C): 100 mM potassium phosphate buffer, pH 6.5, 2.5 mM GSH, and different concentrations of CDNB (22.5–990 µM) in the absence and the presence of inhibitor 4 (20, 40, 60, and 80 µM) or inhibitor 9 (15, 30, and 60 µM) or the control inhibitor BSP (5, 25, and 100 µM),

Kinetic Analysis of Inhibitors 4 and 9 Using GSH as a Variable Substrate. Initial velocities for the hGSTA1-1-catalyzed reaction with GSH as variable substrate were determined in reaction mixtures of a total volume of 1 mL (25 °C): 100 mM potassium phosphate buffer, pH 6.5, 1 mM CDNB, and different concentrations of GSH (40–2475 µM) in the absence and the presence of inhibitor 4 (10, 20, 40, 60, and 80 µM) or inhibitor 9 (15, 30, and 60 µM).

The GraFit3 computer program (Erithacus Software, Ltd., U.K.) was used throughout for producing kinetic graphs and determining apparent kinetic parameters/constants.

■ ASSOCIATED CONTENT

● Supporting Information

Bioactive arylsulfonylpyrroles (Figure SI-1), 3D models of CDNB, GSH, BSP, and the new inhibitors with hGSTA1-1 (Figures SI-2 to SI-4 and SI-5a), enzyme inhibition kinetics (Figures SI-6 to SI-9), HPLC–MS chromatograms of purity analysis (Figure SI-10), and NMR (¹H and ¹³C) and HRMS spectra of compounds 3–11. This material is available free of charge via the Internet at <http://pubs.acs.org>.

■ AUTHOR INFORMATION

Corresponding Author

*For G.I.V.: phone, +30-26510-08382; fax, +30-26510-08799; e-mail, gvarvoun@cc.uoi.gr. For Y.D.C.: phone, +30-210-5294311; fax, +30-210-5294307; e-mail, clonis@aua.gr.

Notes

The authors declare no competing financial interest.

■ ACKNOWLEDGMENTS

We appreciate the use of NMR and mass spectrometry facilities funded by the Network of Research Supporting Laboratories of the University of Ioannina, Greece, and thank Dr. V. Exarchou for 2D NMR spectra, Dr. P. Stathopoulos for low resolution mass spectra, and Dr. V. Boti for high resolution mass spectra. The present work was partly supported by the action “THALIS: Glutathione Transferases, Multifunctional Molecular Tools in Red and Green Biotechnology” falling under the Operational Programme (OP) “Education and Lifelong Learning (EdLL)” and is cofinanced by the European Social Fund (ESF) and National Resources.

■ ABBREVIATIONS USED

BSP, bromosulphophthalein; CDNB, 1-chloro-2,4-dinitrobenzene; DMSO, dimethyl sulfoxide; NBS, *N*-bromosuccinimide; GSH, glutathione; GST, glutathione *S*-transferase; hGSTA1-1, human glutathione *S*-transferase isoenzyme A1-1; IPTG,

isopropyl- β -D-thiogalactopyranoside; mCPBA, 3-chloroperbenzoic acid; MDR, multiple drug resistance

REFERENCES

- (1) Mannervik, B.; Danielson, U. H. Glutathione transferases-structure and catalytic activity. *CRC Crit. Rev. Biochem.* **1988**, *23*, 283–337.
- (2) Armstrong, R. N. Structure, catalytic mechanism and evolution of the glutathione transferases. *Chem. Res. Toxicol.* **1997**, *10*, 2–18.
- (3) Oakley, A. J. Glutathione transferases: new functions. *Curr. Opin. Struct. Biol.* **2005**, *15*, 716–723.
- (4) Frova, C. Glutathione transferases in the genomics era: new insights and perspectives. *Biomol. Eng.* **2006**, *23*, 149–169.
- (5) Oakley, A. J. Glutathione transferases: a structural perspective. *Drug Metab. Rev.* **2011**, *43*, 138–151.
- (6) Sargent, J. M.; Williamson, C.; Hall, A. G.; Elgie, A. W.; Taylor, C. G. Evidence for the involvement of the glutathione pathway in drug resistance in AML. *Adv. Exp. Med. Biol.* **1999**, *457*, 205–209.
- (7) Kodera, Y.; Isobe, K.; Yamauchi, M.; Kondo, K.; Akiyama, S.; Ito, K.; Nakashima, I.; Takagi, H. Expression of glutathione-S-transferases alpha and pi in gastric cancer: a correlation with cisplatin resistance. *Cancer Chemother. Pharmacol.* **1994**, *34*, 203–208.
- (8) Batist, G.; Tulpule, A.; Sinha, B. K.; Katki, A. G.; Myers, C. E.; Cowan, K. H. Over expression of a novel anionic glutathione transferase in multidrug-resistant human-breast cancer cells. *J. Biol. Chem.* **1986**, *261*, 5544–5549.
- (9) Adler, V.; Yin, Z.; Fuchs, S. Y.; Benezra, M.; Rosario, L.; Tew, K. D.; Pincus, M. R.; Sardana, M.; Henderson, C. J.; Wolf, C. R.; Davis, R. J.; Ronai, Z. Regulation of JNK signaling by GSTp. *EMBO J.* **1999**, *18*, 1321–1334.
- (10) Sweeney, C.; Coles, B. F.; Nowell, S.; Lang, N. P.; Kadlubar, F. F. Novel markers of susceptibility to carcinogens in diet: associations with colorectal cancer. *Toxicology* **1988**, *181–182*, 83–87.
- (11) Sau, A.; Trengo, F. P.; Valentino, F.; Federici, G.; Caccuri, A. M. Glutathione transferases and development of new principles to overcome drug resistance. *Arch. Biochem. Biophys.* **2010**, *500*, 116–122.
- (12) Mahajan, S.; Atkins, W. M. The chemistry and biology of inhibitors and pro-drugs targeted to glutathione S-transferases. *Cell. Mol. Life Sci.* **2005**, *62*, 1221–1233.
- (13) Tew, K. D.; Dutta, S.; Schultz, M. Inhibitors of glutathione S-transferases as therapeutic agents. *Adv. Drug Delivery Res.* **1997**, *26*, 91–104.
- (14) Federici, L.; Lo Sterzo, C.; Pezzola, S.; Di Matteo, A.; Scaloni, F.; Federici, G.; Caccuri, A. M. Structural basis for the binding of the anticancer compound 6-(7-nitro-2,1,3-benzoxadiazol-4-ylthio)hexanol to human glutathione S-transferases. *Cancer Res.* **2009**, *69*, 8025–8034.
- (15) Yang, X.; Liu, G.; Li, H.; Zhang, Y.; Song, D.; Li, C.; Wang, R.; Li, B.; Liang, W.; Jing, Y.; Zhao, G. Novel oxadiazole analogues derived from ethacrynic acid: design, synthesis, and structure–activity relationships in inhibiting the activity of glutathione S-transferase P1-1 and cancer cell proliferation. *J. Med. Chem.* **2010**, *53*, 1015–1022.
- (16) Sau, A.; Filomeni, G.; Pezzola, S.; D’Aguanno, S.; Tregno, F. P.; Urbani, A.; Serra, M.; Pasello, M.; Picci, P.; Federici, G.; Caccuri, A. M. Targeting GSTP1-1 induces JNK activation and leads to apoptosis in cisplatin-sensitive and -resistant human osteosarcoma cell lines. *Mol. Biosyst.* **2012**, *8*, 994–1006.
- (17) Wang, C.-H.; Wu, H. T.; Cheng, H. M.; Yen, T.-J.; Lu, I.-H.; Chang, H. C.; Jao, S.-C.; Shing, T. K. M.; Li, W.-S. Inhibition of glutathione S-transferase M1 by new gabosine analogues is essential for overcoming cisplatin resistance in lung cancer cells. *J. Med. Chem.* **2011**, *54*, 8574–8581.
- (18) Findlay, V. J.; Townsend, D. M.; Saavedra, J. E.; Buzard, G. S.; Citro, M. I.; Keller, L. K.; Ji, X.; Tew, K. D. Tumor cell responses to a novel glutathione S-transferase-activated nitric oxide-releasing prodrug. *Mol. Pharmacol.* **2004**, *65*, 1070–1079.
- (19) Axarli, I.; Labrou, N. E.; Petrou, C.; Rassias, N.; Cordopatis, P.; Clonis, Y. D. Sulphonamide-based bombesin prodrug analogues for glutathione transferase, useful in targeted cancer chemotherapy. *Eur. J. Med. Chem.* **2009**, *44*, 2009–2016.
- (20) Pezzola, S.; Antonini, G.; Ceroni, G.; Beria, I.; Colombo, M.; Broggin, M.; Mongelli, N.; Leboffe, I.; MacArthur, R.; Mozzi, A. F.; Federici, G.; Caccuri, A. M. Role of glutathione transferases in the mechanism of brostallicin activation. *Biochemistry* **2010**, *49*, 226–235.
- (21) Johansson, K.; Ito, M.; Schopuizen, C. M. S.; Thengumtharayil, S. M.; Heuse, V. D.; Zhang, J.; Shimoji, M.; Ang, W. H.; Dyson, P. J.; Shibata, A.; Shuto, S.; Ito, Y.; Abe, H.; Morgenstern, R. Characterization of new potential anticancer drugs designed to overcome glutathione transferase mediated resistance. *Mol. Pharmaceutics* **2011**, *8*, 1698–1708.
- (22) Adang, A. E.; Brussee, J.; van der Gen, A.; Mulder, G. J. The glutathione-binding site in glutathione S-transferases. Investigation of the cysteinyl, glycyl and gamma-glutamyl domains. *Biochem. J.* **1990**, *269*, 47–54.
- (23) Morgan, A. S.; Ciaccio, P. J.; Tew, K. D.; Kauvar, L. M. Isozyme-specific glutathione S-transferase inhibitors potentiate drug sensitivity in cultured human tumor cell lines. *Cancer Chemother. Pharmacol.* **1996**, *37*, 363–370.
- (24) Cacciatore, I.; Caccuri, A. M.; Di Stefano, A.; Luisi, G.; Nalli, M.; Pinnen, F.; Ricci, G.; Sozio, P. Synthesis and activity of novel glutathione analogues containing an urethane backbone linkage. *Farmaco* **2003**, *58*, 787–793.
- (25) Adang, A. E.; Moree, W. J.; Brussee, J.; Mulder, G. J.; van der Gen, A. Inhibition of glutathione-S-transferase 3-3 by glutathione derivatives that bind covalently to the active site. *Biochem. J.* **1991**, *278*, 63–68.
- (26) Adang, A. E.; Brussee, J.; van der Gen, A.; Mulder, G. J. Inhibition of rat liver glutathione S-transferase isoenzymes by peptides stabilized against degradation by gamma-glutamyl transpeptidase. *J. Biol. Chem.* **1991**, *266*, 830–836.
- (27) Cacciatore, I.; Caccuri, A. M.; Cocco, A.; De Maria, F.; Di Stefano, A.; Luisi, G.; Pinnen, F.; Ricci, G.; Sozio, P.; Turella, P. Potent isozyme-selective inhibition of human glutathione S-transferase A1-1 by a novel glutathione S-conjugate. *Amino Acids* **2005**, *29*, 255–261.
- (28) Burg, D.; Riepsaame, J.; Pont, C.; Mulder, G.; van der Water, B. Peptide-bond modified glutathione conjugate analogs modulate GSTpi function in GSH-conjugation, drug sensitivity and JNK signaling. *Biochem. Pharmacol.* **2006**, *71*, 268–277.
- (29) Razza, A.; Galili, N.; Smith, S.; Godwin, J.; Lancet, J.; Melchert, M.; Jones, M.; Keck, J. G.; Meng, L.; Brown, G. L.; List, A. Phase 1 multicenter dose-escalation study of ezatiostat hydrochloride (TLK199 tablets), a novel glutathione analog prodrug, in patients with myelodysplastic syndrome. *Blood* **2009**, *113*, 6533–6540.
- (30) McMahon, J. B.; Gulakowsky, R. J.; Weislow, O. S.; Schultz, R. J.; Narayanan, V. L.; Clanton, D. J.; Pedemonte, R.; Wassmundt, F. W.; Buckheit, R. W., Jr.; Decker, C. D.; White, L.; Bader, J. P.; Boyd, M. R. Diarylsulfones, a new chemical class of non-nucleoside antiviral inhibitors of human immunodeficiency virus type 1 reverse transcriptase. *Antimicrob. Agents Chemother.* **1993**, *37*, 754–760.
- (31) Williams, T. M.; Ciccarone, T. M.; MacTough, S. C.; Rooney, C. S.; Balani, S. K.; Condra, J. H.; Emini, E. A.; Goldman, M. E.; Greenlee, W. J. 5-Chloro-3-(phenylsulfonyl)indole-2-carboxamide: a novel, non-nucleoside inhibitor of HIV-1 reverse transcriptase. *J. Med. Chem.* **1993**, *36*, 1291–1294.
- (32) Artico, M.; Silvestri, R.; Stefancich, G.; Massa, S.; Pagnozzi, E.; Musu, D.; Scintu, F.; Pinna, E.; Tinti, E.; La Colla, P. Synthesis of pyrrol aryl sulfones targeted at the HIV-1 reverse transcriptase. *Arch. Pharm. (Weinheim, Ger.)* **1995**, *328*, 223–229.
- (33) Artico, M.; Silvestri, R.; Stefancich, G.; Massa, S.; Loi, A. G.; Corrias, S.; Piras, G.; La Colla, P. 2-Sulfonyl-4-chloroanilino moiety: a potent pharmacophore for the anti-human immunodeficiency virus type 1 activity of pyrrol aryl sulfones. *J. Med. Chem.* **1996**, *39*, 522–530.
- (34) Artico, M.; Silvestri, R.; Pagnozzi, E.; Bruno, B.; Novellino, E.; Greco, G.; Massa, S.; Ettore, A.; Loi, A. G.; Scintu, F.; La Colla, P. Structure-based design, synthesis, and biological evaluation of novel pyrrol aryl sulfones: HIV-1 non-nucleoside reverse transcriptase

inhibitors active at nanomolar concentrations. *J. Med. Chem.* **2000**, *43*, 1886–1891.

(35) Williams, T. M.; Zhang, X.-F.; Obligado, V. E.; Poehnelt, R. A. Non-Nucleoside Reverse Transcriptase Inhibitors. U.S. Patent 2010/0113421 A1, 2007.

(36) Padmavathi, V.; Mahesh, K.; Subbaiah, D. R. C. V.; Deepti, D.; Reddy, G. S. Synthesis and biological activity of a new class of sulfone linked bis(heterocycles). *ARKIVOC* **2009**, *x*, 195–208.

(37) Kalir, A. *o*-Nitrobenzaldehyde. *Org. Synth.* **1973**, *5*, 825–828.

(38) Yadav, J. S.; Reddy, B. V. S.; Shubashree, S.; Sadashiv, K. Iodine/MeOH: a novel and efficient reagent system for thiocyanation of aromatics and heteroaromatics. *Tetrahedron Lett.* **2004**, *45*, 2951–2954.

(39) Kolobe, D.; Sayed, Y.; Dirr, H. W. Characterisation of bromosulphophthalein binding to human glutathione *S*-transferase A1-1: thermodynamics and inhibition kinetics. *Biochem. J.* **2004**, *382*, 703–709.

(40) Lu, Y.; Shi, T.; Wang, Y.; Yang, H.; Yan, X.; Luo, X.; Jiang, H.; Zhu, W. Halogen bonding: a novel interaction for rational drug design? *J. Med. Chem.* **2009**, *52*, 2854–2862.

(41) Hernandez, M. Z.; Cavalcanti, S. M.; Moreira, D. R.; de Azevedo Junior, W. F.; Leite, A. C. Halogen atoms in the modern medicinal chemistry: hints for the drug design. *Curr. Drug Targets* **2010**, *11*, 303–314.

(42) Jorgensen, W. L.; Duffy, E. M. Prediction of drug solubility from Monte Carlo simulations. *Bioorg. Med. Chem. Lett.* **2000**, *10*, 1155–1158.

(43) Jorgensen, W. L.; Duffy, E. M. Prediction of drug solubility from structure. *Adv. Drug Delivery Rev.* **2002**, *54*, 355–366.

(44) Roberts, D. V. *Enzyme Kinetics*; Cambridge University Press: Cambridge, U.K., 1977; pp 49–58, 65–69.

(45) Dixon, M.; Webb, E. *Enzymes*, 3rd ed.; Longman Group Ltd.: London, U.K., 1979; pp 332–381.

(46) Leskovac, V. *Comprehensive Enzyme Kinetics*; Kluwer Academic Publishers: New York, U.S., 2003; pp 73–110, 139–170.

(47) Sluis-Cremer, N.; Wallace, L.; Burke, J.; Stevens, J.; Dirr, H. W. Aflatoxin B1 and sulphobromophthalein binding to the dimeric human glutathione *S*-transferase A1-1: a fluorescence spectroscopic analysis. *Eur. J. Biochem.* **1998**, *257*, 434–442.

(48) Sayed, Y.; Hornby, J. A.; Lopez, M.; Dirr, H. Thermodynamics of the ligandin function of human class alpha glutathione *S*-transferase A1-1: energetics of organic anion ligand binding. *Biochem. J.* **2002**, *363* (Part 2), 341–346.

(49) Sluis-Cremer, N.; Naidon, N. N.; Kaplan, W. H.; Monoharan, T. H.; Fahl, W. E.; Dirr, H. W. Determination of a binding site for non-substrate ligand in mammalian cytosolic glutathione *S*-transferase by means of fluorescence-resonance energy transfer. *Eur. J. Biochem.* **1996**, *241*, 484–488.

(50) Grah, E.; Novotny, M.; Jakobsson, E.; Gustafsson, A.; Grehn, L.; Olin, B.; Madsen, D.; Wahlberg, M.; Mannervik, B.; Kleywegt, G. J. New crystal structures of human glutathione transferase A1-1 shed light on glutathione binding and the conformation of the C-terminal helix. *Acta Crystallogr., Sect. D: Biol. Crystallogr.* **2006**, *62*, 197–207.

(51) Leonard, J.; Lygo, B.; Procter, G. *Advanced Practical Organic Chemistry*; Nelson Thornes Ltd.: Cheltenham, U.K., 2001.

(52) Still, W. C.; Kahn, M.; Mitra, A. Rapid chromatographic technique for preparative separations with moderate resolution. *J. Org. Chem.* **1978**, *43*, 2923–2925.

(53) Sanner, M. F. Python: a programming language for software integration and development. *J. Mol. Graphics Modell.* **1999**, *17*, 57–61.

(54) Morris, G. M.; Goodsell, D. S.; Halliday, R. S.; Huey, R.; Hart, W. E.; Bewley, R. K.; Olson, A. J. Automated docking using a Lamarckian genetic algorithm and an empirical binding free energy function. *J. Comput. Chem.* **1998**, *19*, 1639–1662.

(55) Cornell, W. D.; Cieplak, P.; Bayly, C. I.; Gould, I. R.; Merz, K. M., Jr.; Ferguson, D. M.; Spellmeyer, D. C.; Fox, T.; Caldwell, J. W.; Kollman, P. A. A second generation force field for the simulation of

proteins, nucleic acids, and organic molecules. *J. Am. Chem. Soc.* **1995**, *117*, 5179–5197.

(56) DeLano, W. L. The PyMOL molecular graphics system on World Wide Web, 2004, available at <http://www.pymol.org>.

(57) Paumi, C. M.; Smitherman, P. K.; Townsend, A. J.; Morrow, C. S. Glutathione *S*-transferases (GSTs) inhibit transcriptional activation by the peroxisomal proliferator-activated receptor gamma (PPAR gamma) ligand, 15-deoxy-delta(12,14)prostaglandin J(2) (15-d-PGJ(2)). *Biochemistry* **2004**, *43*, 2345–2352.